Learning Cognitive Map Representations for Navigation by Sensory–Motor Integration

Dongye Zhao, Zheng Zhang, Hong Lu, *Member, IEEE*, Sen Cheng, Bailu Si, *Member, IEEE*, and Xisheng Feng

***Abstract*—How to transform a mixed flow of sensory and motor information into memory state of self-location and to build map representations of the environment are central questions in the navigation research. Studies in neuroscience have shown that place cells in the hippocampus of the rodent brains form dynamic cognitive representations of locations in the environment. We propose a neural-network model called sensory–motor integration network model (SeMINet) to learn cognitive map representations by integrating sensory and motor information while an agent is exploring a virtual environment. This biologically inspired model consists of a deep neural network representing visual features of the environment, a recurrent network of place units encoding spatial information by sensorimotor integration, and a secondary network to decode the locations of the agent from spatial representations. The recurrent connections between the place units sustain an activity bump in the network without the need of sensory inputs, and the asymmetry in the connections propagates the activity bump in the network, forming a dynamic memory state which matches the motion of the agent. A competitive learning process establishes the association between the sensory representations and the memory state of the place units, and is able to correct the cumulative path-integration errors. The simulation results demonstrate that the network forms neural codes that convey location information of the agent independent of its head direction. The decoding network reliably predicts the location even when the movement is subject to noise. The proposed SeMINet thus provides a brain-inspired neural-network model for cognitive map updated by both self-motion cues and visual cues.**

***Index Terms*—Cognitive map, hippocampus, navigation, path integration, place cells, self-motion cues, sensorimotor integration, sensory–motor integration network model (SeMINet), visual cues.**

Manuscript received July 31, 2018; revised April 21, 2019 and December 14, 2019; accepted February 25, 2020. Date of publication April 3, 2020; date of current version January 10, 2022. The work of Bailu Si was supported by the National Key Research and Development Program of China under Grant 2016YFC0801808. The work of Sen Cheng was supported by the German Research Foundation through SFB 1280, Project A14. This article was recommended by Associate Editor A. Katriniok. *(Corresponding author: Bailu Si.)*

Dongye Zhao is with the State Key Laboratory of Robotics, Shenyang Institute of Automation, Chinese Academy of Sciences, Shenyang 110016, China, also with the Institutes for Robotics and Intelligent Manufacturing, Chinese Academy of Sciences, Shenyang 110169, China, and also with the University of Chinese Academy of Sciences, Beijing 100049, China (e-mail: zhaodongye@sia.cn).

Zheng Zhang is with the Department of Computer Science, New York University Shanghai, Shanghai 316021, China (e-mail: zz@nyu.edu).

Hong Lu is with the School of Computer Science, Fudan University, Shanghai 200433, China (e-mail: honglu@fudan.edu.cn).

Sen Cheng is with the Institute for Neuroinformatics, Ruhr-Universität Bochum, 44801 Bochum, Germany (e-mail: sen.cheng@rub.de).

Bailu Si is with the School of Systems Science, Beijing Normal University, Beijing 100875, China (e-mail: bailusi@bnu.edu.cn).

Xisheng Feng is with the State Key Laboratory of Robotics, Shenyang Institute of Automation, Chinese Academy of Sciences, Shenyang 110016, China, and also with the Institutes for Robotics and Intelligent Manufacturing, Chinese Academy of Sciences, Shenyang 110169, China (e-mail: fxs@sia.cn).

Color versions of one or more figures in this article are available at https://doi.org/10.1109/TCYB.2020.2977999.

Digital Object Identifier 10.1109/TCYB.2020.2977999

I. Introduction

TO NAVIGATE in space, an agent must possess a range of generic cognitive abilities, such as perception, memory, and action execution. One specific and essential feature required for spatial navigation is a cognitive map of the environment, which can be used to optimize the actions of the agent over a long time scale and large spatial range. For instance, a cognitive map is required for path planning [1], route following [2], and homing [3]. To build a cognitive map of an unknown environment without external location information such as GPS, the agent has to infer its location and incrementally construct the map from its own sensory and motor information, a problem called simultaneous localization and mapping (SLAM) [4]. When performing SLAM, the flow of sensorimotor information is transformed into memory states of self-locations and a cognitive map representation of the environment is constructed.

Classical engineering solutions to the SLAM problem rely on filtering methods, such as extended Kalman filter and particle filter [5], [6]. Filtering-based methods formulate the SLAM problem in a state-space framework. The motion of the agent is described by a state transition equation, and the sensory information, mostly from laser rangefinders, is incorporated to update the state using the Bayes rule. Filtering-based methods provide beautiful mathematical frameworks for SLAM, however, they are challenged in terms of robustness and scalability when applied to large-scale dynamic environments. In dynamic environments, it is hard to associate perception with internal representations. Incorrect data association (i.e., the mismatch between perception and internal representations) can often lead the filter algorithm into irreversible divergence. Filtering-based methods assume static motion dynamics of the agent, and are not able to adapt to dynamic changes such as varying working conditions.

As an alternative to filtering-based SLAM methods, neural-network models have been adopted to tackle the SLAM problem [7], [8]. Neural networks form distributed

representations of the environment and learning often take place locally in the network connections. These mechanisms prevent neural networks from sudden divergence and allow networks to adapt to the environment incrementally. Neural-network models of SLAM are motivated by the behavioral and neurobiological studies on the spatial memory circuits of mammalian brains. Animals efficiently acquire cognitive maps of novel environments and learn to accurately navigate to specific goals. Indeed, neuroscientific studies found that mammals, such as rats, have an "Inner GPS" in their brains [9]. Certain neurons within the hippocampus are activated as the rat visits specific regions of the environment (so-called place fields) [10]. This kind of spatially selective neurons, called place cells, is the embodiment of the cognitive map [11], [12]. Place cells in the hippocampus interact extensively with other cells that represent spatial information, such as grid cells and head-direction cells in the entorhinal cortex (EC) [13]. Hippocampus, EC, and related cortices form a spatial navigation network, the "Inner GPS," which allows mammals to navigate large and dynamically changing natural environments. Can robotic navigation systems benefit from insights into the biological mechanisms of navigation? Neuroscientists and roboticists have commenced to develop biologically plausible models for robot navigation [14]–[21]. For example, Müller *et al.* [14] proposed the "cognitive graph" model for encoding, in the synaptic weights between place cells, the spatial distance between certain locations in the environment represented by the place cells firing. Samsonovich and McNaughton [15] proposed a neural network architecture with a motor system and sensory system, which encodes movement and spatial location, to explain mechanisms of mammalian path integration in a continuous attractor network. In [16], a place cell model for combining perceptual features and path integration cues by means of a competitive Hebbian learning rule was proposed, and accounted for the diversity of place cell responses. Banino *et al.* [21] proposed a supervised recurrent network to perform path integration, in which multiscale periodical representations similar to grid cells activity emerged. These representations were further shown to be critical for vector-based navigation in the challenging and unfamiliar environments. Sitting on the top of the deep hierarchy of the sensory processing pathways [22], the hippocampus integrates multiple types of highly processed sensory information to form a new episodic memories. Memory is not just an isolated module of brain functions, it is tightly coupled with and plays a critical role in perception, learning, and decision making. However, most existing models of cognitive maps do not consider the hierarchical nature of perception, and simply assume highly idealized features as the inputs to the memory model [15], [16], [23], [24].

Motivated by the distributed hierarchical processing of the visual cortex, deep neural networks have been developed to mimic the hierarchical architecture of visual information processing in the brain. Deep neural networks transform high-dimensional complex sensory data into concise representations of visual features and tremendously boost the performance of recognition and classification. In this article, we propose a sensory–motor integration network model (SeMINet) of the hippocampal cognitive map. The novelty of this article is two-fold. First, we model the perception and memory in a unified integrated framework. Second, the network model is biologically plausible, in that the connectivity of the network model is based on the findings of the anatomical organization of the spatial memory circuits in mammalian brains. We reproduce some of the key properties of place cells observed in neurobiological studies.

The proposed network model is inspired by the brain cognitive architecture and computational mechanisms. Theoretical studies have shown that neural networks are able to implement Bayesian information integration [25], [26]. It is, therefore, possible to constrain the network activity in probability space and perform the probabilistic computation for navigation like what filtering-based SLAM methods do. In this article, however, we do not intend to provide a solution for robot navigation in real-world environments. Instead, we focus on the biological plausibility and show that, with simple sensor data, an integrated perception-memory model is able to learn stable representations for spatial cognition. To this end, we follow [27] and set a virtual agent (rat or robot) in a simulated box maze, a common environment setup in neurobiological experiments.

II. Materials and Methods

A. Network Architecture

To develop a biologically plausible model of the hippocampus for navigation, it is essential to lay down the foundation based on the key properties of the spatial memory circuit. We list several salient features of the hippocampus in the following.

1) The hippocampus receives projections from the lateral EC (LEC) and the medial EC (MEC). LEC cells encode information about objects and context [28]. MEC contains grid cells that encode the conjunction of space and movement, and speed cells and head-direction cells that encode the speed and the head direction of the animal.
2) In the ventral visual system of rats, neurons in the inferior temporal cortex form invariant representations of visual objects, which are the main inputs to the hippocampal system relayed by the LEC [29], [30]. As described by [31], the Hebbian-like learning rule incorporating the previous activity of cells may be the biological mechanism for learning invariant visual representations.
3) Besides visual cues, electrophysiology recordings show that place cells perform path integration based on self-motion cues in the absence of visual cues, that is, in the dark [32]. When available, visual stimuli merely modulate the firing rates of place cells in rats [33]–[36]. Therefore, it appears that place cells activity is driven by self-motion cues and visual stimuli serve to correct the movement errors [37], [38].
4) In the CA3 region of the hippocampus, there are strong recurrent connections between place cells [15], [24]. These recurrent connections form an attractor network and encode movement sequences.

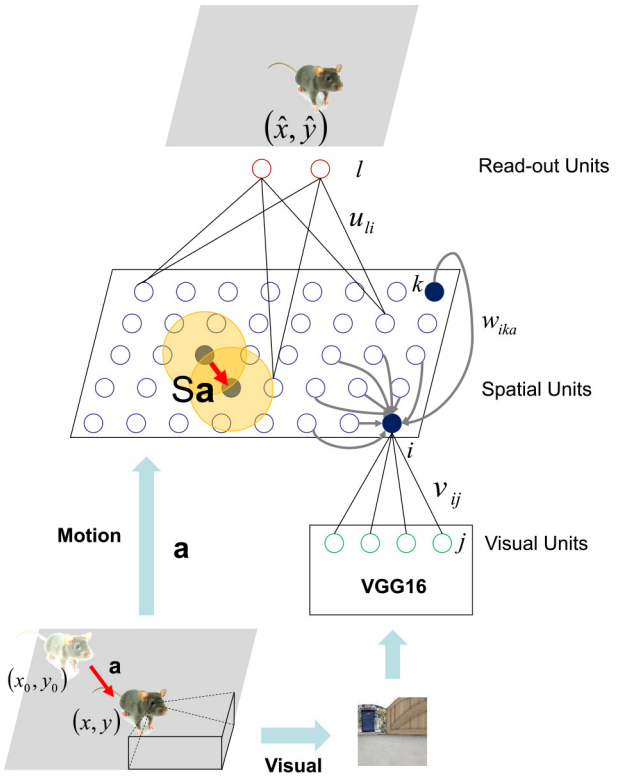

Fig. 1. Framework of the SeMINet model. The architecture has two perceptual inputs: visual cues and self-motion cues. The image of the visual scene is presented to the input layer of the pretrained VGG16 network. The 18th layer of the pretrained VGG16 network consists of 8192-visual units (*green circles*), and are connected to the 1500-spatial units (*blue circles*) in the hippocampus. The activity of the spatial units is decoded by two read-out units (*red circles*) representing the x–y coordinates of the robot in the environment. Each layer is fully connected to the next layer (*black lines*). Recurrent connections w_{ika} (*gray lines with arrows*) represent the synaptic strength from spatial units k to unit i when the robot moves with velocity $\boldsymbol{a}$. The activity of spatial units would converge to an activity bump (*highlighted yellow disk*) through recurrent connections. The velocity inputs $\boldsymbol{a}$ with a positive scaling factor S propagate the center of the bump.

Based on these properties, we develop a network model of the hippocampus with the perception-memory architecture called SeMINet (Fig. 1). In the model, the hippocampus consists of a layer of interconnected place units. The place units receive two types of perceptual inputs and form memories of the positions of the robot in the environment. The visual inputs are relayed by a deep neural network, namely, a pretrained VGG16 network consisting of 18 layers. The deep neural network extracts visual features from the input images, mimicking the ventral visual pathway, and its output layer serves as a model of LEC. Motion information can be decoded from MEC, but in our model, it is directly fed to the place units for simplicity. In order to evaluate the quality of the spatial memory formed in the place units, we use a decoding network based on predictive learning to read out the spatial code of place units.

B. Cognitive Map Representations

To encode positions in 2-D environments, we assume that the spatial units in the hippocampus are arranged regularly on an abstract 2-D neural space with size $\ell_x \times \ell_y$ of arbitrary units. We use $\ell_x = 50$ and $\ell_y = 30$. Spatial units are arranged on a 50×30 rectangular grid, with equal distance between neighboring units, resulting in 1500 spatial units in total (Fig. 1). To avoid boundary effects, the neural space has periodic boundary conditions [39], that is, units at the edges of the neural space connect to units on the opposite sides. Periodic boundaries turn the flat 2-D neural space into a torus.

The spatial units integrate both visual information and velocity information. The firing rate h_i of spatial unit i is given by

$$h_i(t) = \left[I_i^m(t) + \rho I_i^v(t) + I\right]^+ \tag{1}$$

where $[\cdot]^+$ is the threshold-linear transfer function, I^m is the velocity inputs, I^v is the visual inputs, $\rho = 0.5$ is the strength of the visual input, and I is the threshold of the spatial unit activity, set to 10.

The visual input to the spatial unit i is

$$I_i^v(t) = \frac{1}{M} \sum_j v_{ij}(t-1) f_j(t) \tag{2}$$

where f_j is the firing rate of visual unit j in the output layer of the deep neural network, v_{ij} is the synaptic strength from visual unit j to spatial unit i, and M is the number of visual units.

The recurrent input to the spatial unit i is

$$I_i^m(t) = \frac{1}{N} \sum_k w_{ika}(t) h_k(t-1) \tag{3}$$

where h_k is the firing rate of spatial unit k, w_{ika} is the recurrent connection strength from spatial unit k to spatial unit i when the velocity of the robot is a, and N is the number of spatial units.

The recurrent connection w_{ika} is defined as

$$w_{ika}(t) = J_1 \exp\left(-\frac{\|D(\boldsymbol{\Theta}_i, \boldsymbol{\Theta}_k + S\boldsymbol{a}(t))\|^2}{2\sigma_m^2}\right) - J_0. \tag{4}$$

$\boldsymbol{\Theta}_i = (\theta_i^1, \theta_i^2)$ is the coordinate of unit i on the neural torus. $\theta_i^1 \in [0, \ell_x)$ and $\theta_i^2 \in [0, \ell_y)$ are regularly distributed on a rectangular grid with periodic boundary conditions. $\|\boldsymbol{x}\| = \sqrt{\sum_k x_k^2}$ is the length of a vector $\boldsymbol{x}$, with x_k as the elements of the vector. $D(\cdot, \cdot)$ takes the difference between two points on the torus in each dimension, respectively

$$D(\boldsymbol{\Theta}_i, \boldsymbol{\Theta}_k) = \begin{pmatrix} \mathrm{mod}\left(\theta_i^1 - \theta_k^1 + \frac{\ell_x}{2}, \ell_x\right) - \frac{\ell_x}{2}, \\ \mathrm{mod}\left(\theta_i^2 - \theta_k^2 + \frac{\ell_y}{2}, \ell_y\right) - \frac{\ell_y}{2} \end{pmatrix}^{\mathrm{T}}. \tag{5}$$

$\mathrm{mod}(\cdot, \cdot)$ is the modulo operation defined for real numbers. T is the transpose of a vector. σ_m is the spread of spatial tuning. $J_1 = 78$ and $J_0 = 2.3$ are the excitatory and inhibitory strength of the connections, respectively. $\boldsymbol{a}(t)$ is the velocity input to the network. $S > 0$ is a positive scaling factor, set to 0.5. The recurrent connections can be formed during the postnatal development stage by Hebbian type of learning, which lead the activity of spatial units to converge to a localized activity packet called "activity bump," an attractor state of the network [15], [40]. The velocity inputs modulate the center of the recurrent connections. For example, if the robot stands still, that is, the velocity input $\boldsymbol{a}(t) = 0$, the postsynaptic cell that is maximally activated by the presynaptic cell $\boldsymbol{\Theta}_k$ is itself,

that is, the recurrent connection profile is centered at $\mathbf{\Theta}_k$. The velocity-dependent recurrent connection profile gives a simple mechanism of path integration. A more biologically plausible solution would require conjunctive representations of velocity and position [15], [17].

C. Learning of Feedforward Connections

The feedforward connections from visual units to spatial units are adapted according to the following learning rule:

$$v_{ij}(t) = v_{ij}(t-1) + \eta \bar{h}_i(t-1) f_j(t) \tag{6}$$

where h_i is the firing rate of the spatial unit i, $\eta = 0.0005$ is a positive learning rate, and $\bar{h}_i(t)$ is obtained by averaging the activity of the spatial unit i

$$\bar{h}_i(t) = (1-\epsilon) h_i(t) + \epsilon \bar{h}_i(t-1). \tag{7}$$

Here, $\epsilon \in (0, 1)$ is a positive averaging factor, and we used $\epsilon = 0.6$ in the experiments. $\bar{h}_i$ represents a trace of the firing rate of unit i. The weight update in (6) is called the trace rule [41], it facilitates the association of the postsynaptic activity to the presynaptic patterns in a long time scale, and therefore helps extract invariant features from the efferent inputs.

At each time step, weights are further normalized into the unitary length $\sum_j {v_{ij}}^2(t) = 1$.

D. Position Prediction

The activity of the spatial units forms neural codes of the 2-D environment. In order to evaluate the coding accuracy of the neural codes, we construct a simple decoding network to read out the positional information from the spatial units.

The location of the robot is predicted by

$$\hat{r}_l(t) = \sum_i u_{li}(t-1) h_i(t) \tag{8}$$

where $u_{li}(t)$ is the connection from the spatial unit i to the read-out unit l, and $l \in \{1, 2\}$ represents the two dimensions of the predicted position $\hat{r}$.

The prediction error $E(t)$ is given by the L_2 norm of the difference between the actual position $r(t)$ and the predicted position $\hat{r}(t)$

$$E(t) = \frac{1}{2} \sum_l \big(r_l(t) - \hat{r}_l(t)\big)^2. \tag{9}$$

The connection u is learned by stochastic gradient descent (SGD) with the learning rate $\gamma = 0.0001$

$$u_{li}(t) = u_{li}(t) - \gamma \frac{\partial E(t)}{\partial u_{li}(t)} \tag{10}$$

where the gradient is

$$\frac{\partial E(t)}{\partial u_{li}(t)} = -\big(r_l(t) - \hat{r}_l(t)\big) h_i(t). \tag{11}$$

E. Estimation of the Bump Location

The population activity of the spatial units comprises an encoding of the location of the robot in the environment. The spatial codes can be extracted from the population activity of the spatial units. We define the following transformations of the activity h to characterize the amplitude A and the positional phase ψ of the bump in the neural space:

$$A_1 \exp(j\psi_1(t)) \coloneqq \frac{1}{N} \sum_k h_k(t) \exp\left(j \frac{2\pi\theta_k^1}{\ell_x}\right) \tag{12}$$

$$A_2 \exp(j\psi_2(t)) \coloneqq \frac{1}{N} \sum_k h_k(t) \exp\left(j \frac{2\pi\theta_k^2}{\ell_y}\right). \tag{13}$$

(θ_k^1, θ_k^2) is the coordinate of unit k on the neural torus. j here indicates the imaginary unit. According to the definitions in (12) and (13), the phases $\psi_1(t)$ and $\psi_2(t)$ are in the range $[0, 2\pi)$, and represent the center of the activity profile considering each side of the torus as circular dimensions. By scaling, the position of the activity profile on the neural space is then estimated as

$$\boldsymbol{\xi}(t) = \left(\frac{\psi_x(t)\ell_x}{2\pi}, \frac{\psi_y(t)\ell_y}{2\pi}\right). \tag{14}$$

And the velocity of the bump is

$$\boldsymbol{v}(t) = \frac{D(\boldsymbol{\xi}(t), \boldsymbol{\xi}(t-1))}{\Delta t} \tag{15}$$

where $D(\cdot, \cdot)$ is defined in (5). Here, Δt is the time interval between two time steps.

III. Characterization of Place Codes

To reveal the information conveyed by the activity of the spatial units in the network, we quantitatively measure the characteristics, such as the directional selectivity, continuity, and the information content, of the place codes in the framework of probability. The probability measure allows evaluation of models without relying on algorithmic details, therefore, could serve an objective evaluation of models of different nature. In this article, we construct probability distributions from network activity, and adopt information-theoretic tools to measure the place codes learned by the network. Our characterization method could be used by both robotic and neuroscience research.

More specifically, the firing activity of each spatial unit is binned to obtain firing maps $m(x)$, $m(\alpha)$, and $m(x; \alpha)$ as a function of location bin x, head-direction bin α, and conjunction of locations and head directions, respectively. For simplicity, we neglect the indices of the spatial units in this section.

A. Information of Place Cell Activity

The spatial information conveyed by the place fields of a unit can be measured by the mutual information between the firing activity of a unit and the spatial location. The spatial information rate, that is, the spatial information per unit time, of a spatial unit is given by

$$I_p = \frac{1}{N_p} \sum_x m(x) \log_2 \frac{m(x)}{\bar{m}_p} \tag{16}$$

where $\bar{m}_p = \sum_x m(x)/N_p$. N_p is the number of location bins. The spatial information rate is derived by assuming uniform occupancy of locations in the environment [42]. The detailed derivation is given in the Appendix for the sake of

TABLE I
VELOCITY VECTORS OF THE MOVEMENTS OF THE ROBOT

Movement	v_x (m/s)	v_y (m/s)	Movement	v_x (m/s)	v_y (m/s)
N	0	1	NE	$\frac{\sqrt{2}}{2}$	$\frac{\sqrt{2}}{2}$
S	0	-1	NW	$-\frac{\sqrt{2}}{2}$	$\frac{\sqrt{2}}{2}$
E	1	0	SW	$-\frac{\sqrt{2}}{2}$	$-\frac{\sqrt{2}}{2}$
W	-1	0	SE	$\frac{\sqrt{2}}{2}$	$-\frac{\sqrt{2}}{2}$

completeness. The uniform occupancy is only a convenient assumption for the evaluation of the network. During learning, the uniform occupancy is not required. For the general case of arbitrary occupancy distribution, the spatial information rate is computed by including the occupancy explicitly (27).

In a similar way, the directional information rate of the firing activity of the units is given by

$$I_d = \frac{1}{N_d} \sum_{\alpha} m(\alpha) \log_2 \frac{m(\alpha)}{\bar{m}_d} \tag{17}$$

where $\bar{m}_d = \sum_{\alpha} m(\alpha)/N_d$, with N_d being the number of direction bins.

B. Selectivity in Head Direction

To determine the degree to which the activity of a spatial unit changes with respect to the head directions of the robot, we use the Rayleigh vector length R [43] as an indicator, which is computed as the modulus of the complex number representing the average direction weighted by the activities of a spatial unit

$$R \exp(j\phi) := \frac{\sum_{\alpha} m(\alpha) \exp(j\alpha)}{\sum_{\alpha} m(\alpha)} \tag{18}$$

where j is the imaginary unit. $m(\alpha)$ is the mean activity of a spatial unit in head-direction bin α. The length $R \in [0, 1]$ measures the head-direction selectivity of the spatial unit. The larger the length R, the more the concentrated of the activity around the preferred direction ϕ.

C. Consistency

To quantify the invariance of place fields with respect to head directions, we calculate the consistency of the place fields by averaging the distance between place codes expressed in different directions

$$C = \frac{1}{2N_d(N_d-1)} \sum_{1 \le i \ne k \le N_d} \left[D_{KL}\left(q(x;\alpha_i) \middle\| \frac{q(x;\alpha_i)+q(x;\alpha_k)}{2} \right) + D_{KL}\left(q(x;\alpha_k) \middle\| \frac{q(x;\alpha_i)+q(x;\alpha_k)}{2} \right) \right] \tag{19}$$

where $q(x;\alpha_i)$ is the firing likelihood of a spatial unit in location bin x given head-direction bin α_i (i.e., $q(x;\alpha_i) = m(x;\alpha_i)/\sum_x m(x;\alpha_i)$ is the normalized firing activity of the spatial unit). N_d is the number of head-direction bins. $D_{KL}(q(x;\alpha_i)||q(x;\alpha_k))$ is the Kullback–Leibler divergence between the firing likelihood of the spatial unit in two head-direction bins

$$D_{KL}(q(x;\alpha_i)\|q(x;\alpha_k)) = \sum_x q(x;\alpha_i) \log_2 \frac{q(x;\alpha_i)}{q(x;\alpha_k)}. \tag{20}$$

A large value of C indicates different firing fields when the robot faces different head directions, that is, low consistency of place fields in head directions, while zero value of C means that the spatial unit fires in the same way for all head directions, that is, maximal consistency of place fields.

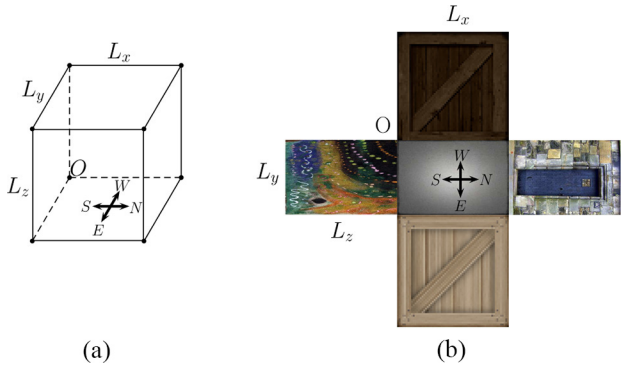

Fig. 2. Simulated virtual environment. (a) Box maze, with the size of 60 m (L_x) × 40 m (L_y) × 60 m (L_z), has four walls and one floor. (b) Expanded view from the top of the textures of the walls and the floor. N: North; S: South; E: East; and W: West.

IV. EXPERIMENTS

We simulate a robot navigating in a virtual box maze with the size of 60 m × 40 m × 60 m in length, width, and height, respectively (Fig. 2). The simulation environment is from the RatLab described in [44]. The simulation consists of a learning phase and a testing phase. In the learning phase, the virtual robot randomly explores the maze with a continuous trajectory while the network learns a representation of the environment. The speed of the robot is fixed at 1 m/s. One simulation step corresponds to one second in time. For simplicity, the movement of the robot is restricted to eight possible directions, namely, north, south, west, east, northeast, northwest, southeast, and southwest. At each time, the robot chooses among its current direction and the two adjacent directions with 45° separation with equal probabilities. To avoid collision with the wall, the robot keeps a distance to the wall ≥ 5 m. This is achieved by choosing a movement direction parallel to or away from the wall when it is about to move too close to a wall. Table I summarizes the velocities of the movement steps. To simulate a natural situation where

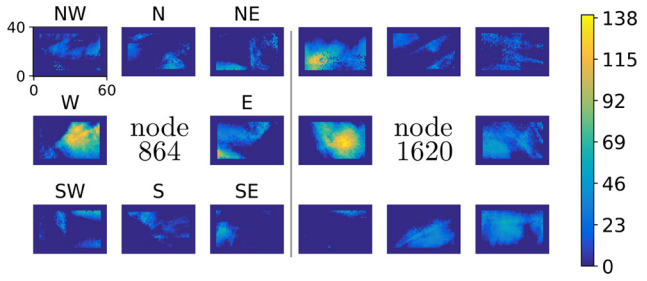

Fig. 3. Response of visual units is weakly selective in space and does not show coherent selectivity in head directions. The activity of two example visual units is shown in separate quadrants. Each panel displays the activity of a unit in space for different head directions, with yellow color for high activity and blue color for zero activity.

the mammal has only a frontal view, the head direction of the robot is the same as the movement direction during the entire simulation. The visual input to the robot is an image of size 128 pixels $\times$ 128 pixels, and is fed to the visual network. The learning phase lasts for 20-learning epochs, each of which lasts for 20 000 time steps. After the learning phase, we simulate a testing phase, in which the network stops adapting its connections. Note that in the testing phase, the virtual robot takes the same exploring rule as it does in the learning phase.

A. Visual Features

When the robot faces some particular directions, the activity of visual units has peaks in certain locations of the environment, and decays slowly and smoothly in space (ref. panels in Fig. 3). Thus, the response of visual units is weakly selective in space. This is because visual units have learned to represent specific visual features, and visual features in natural scenes change continuously in the environment. Other than the fact that the activity of visual units varies slowly in space, the activity of visual units changes more rapidly as a function of direction. This is largely due to the fact that the field of view (FOV) of the robot camera is rather limited.

B. Cognitive Map Representation

The activity of the spatial units is initialized randomly before the simulation starts. Due to the recurrent connections between the spatial units, a localized activity pattern emerges in the neural space [Fig. 4(a)]. The emergence of the activity bump is determined by the symmetry-breaking process of pattern formation [45]. The strength of visual inputs fed into the network is $\rho = 0.5$. During learning, the network learns the feedforward connections from visual units to spatial units according to the trace rule. The learning process establishes the association between the visual inputs and the network state. After an initial transient period of about 170 time steps, the activity pattern is stabilized at a constant activity level [Fig. 4(b)].

With sensorimotor integration, spatial units form firing fields in the environment [Fig. 5(a)]. The firing fields of each active unit are localized and cover part of the environment. The firing fields of different spatial units are scattered across the environment, tiling the whole environment. The firing fields expressed in different head directions are independent of the head directions, and the maximal firing rate of spatial units is

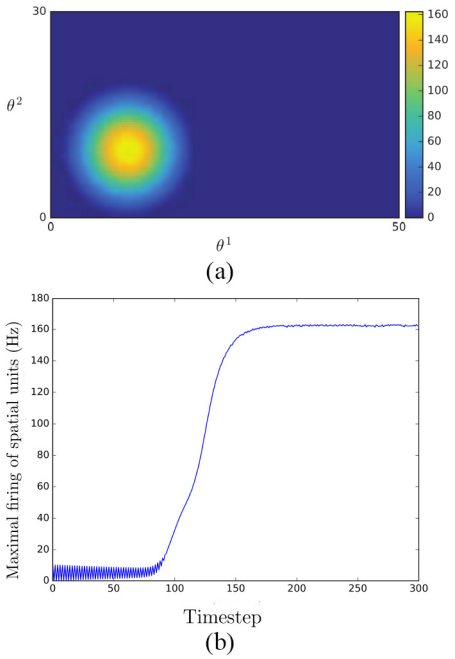

Fig. 4. Population activity of the spatial units. (a) Localized activity bump emerges in the network. $\ell_x = 50$ and $\ell_y = 30$. The activity of the spatial units is colored by yellow for high activity and blue for zero activity. Only a fraction of spatial units is activated, forming a Gaussian-shaped bump on the 2-D neural space. The center/peak of the bump encodes the robot position in the environment. (b) Peak activity of the spatial units converges to a stable state after about 170 time steps. $J_1 = 78$, $J_0 = 2.3$, $\sigma_m = 2$ [ref. (4)].

similar for all head directions [Fig. 5(b)]. Therefore, the firing fields of the spatial units are invariant to head directions. These characteristics of the place codes of the spatial units in the model are consistent with the characteristics of the place fields observed in open field experiments, in which rats perform random exploration. Collectively, the spatial units in the model form a cognitive map representation of the environment.

To quantify the characteristics of the place codes of the network, we measure the information content, selectivity, and consistency of the firing maps of the spatial units (see Section III).

A large fraction of the spatial units has high spatial information rate I_p [Fig. 6(a)]. About half of the spatial units show a very low spatial information rate due to the fact that these units are not active in the environment or are activated only in a very small area near the border of the environment. In terms of the directional information rate, the spatial units convey almost zero information on the head direction [Fig. 6(b)]. The joint scattering of spatial information and directional information reveals that the directional information is distributed in a very narrow range and the positional information covers a wide range [Fig. 6(c)]. This demonstrates conclusively that the firing rate of spatial units conveys location information, but not directional information. This is consistent with earlier work that place cells mainly express spatial information, not other information such as context [46]. More quantitatively, our result shows that on average CA3 place cells encode position with about 14 b/s, or 0.0875 b/spike after normalized by the peak firing rate. This result roughly falls in the same range of place cell activity observed experimentally

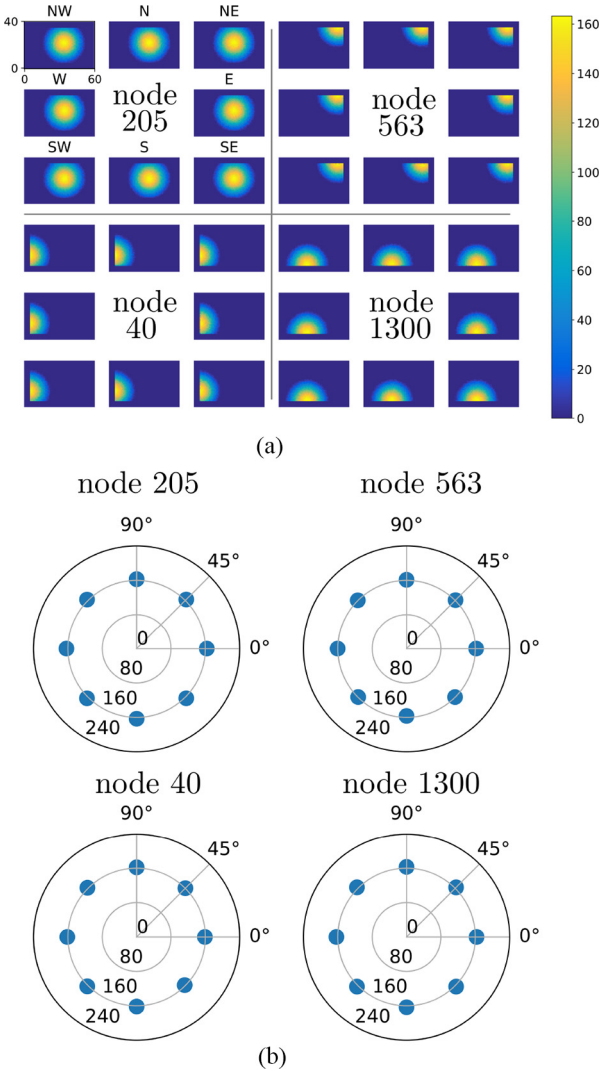

Fig. 5. Spatial units in the network form localized firing fields in the environment. (a) Activity of four example spatial units is shown in separate quadrants. Each panel displays the activity of a unit in space for different head directions. The activity is coded according to the color bar on the right, with yellow color for high activity and blue color for zero activity. Spatial units show localized firing fields in space. The firing fields of the same spatial unit in different head directions are centered at the same location. (b) Maximal firing rate of each spatial unit in different head directions is invariant.

by [47]. They showed that the amount of spatial information conveyed by hippocampal neurons is about 2.02 b/s, or about 0.02 b/spike if normalized by the peak firing rate.

Another method for investigating a directional bias is the Rayleigh vector length. The activity of spatial units has very low Rayleigh vector length [Fig. 7(a)], meaning that spatial units do not fire preferentially when the rat moves in a particular head direction. This is consistent with the fact that the spatial units do not convey directional information [Fig. 6(b)]. The joint distribution of the Rayleigh vector length and directional information is concentrated near the origin [Fig. 7(b)]. The low values of direction selectivity R and directional information I_d prove that these two measures are equally valid in describing the directional responses of neurons. However, the shape of the distribution implies that the relationship between the two measures is nonlinear [Fig. 7(b)].

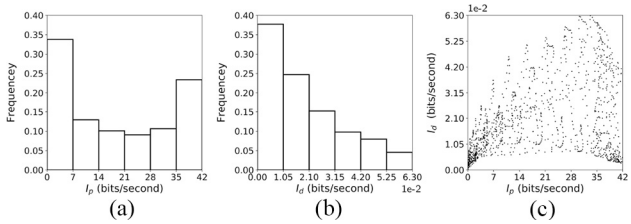

Fig. 6. Information conveyed by the spatial units is purely positional. (a) Proportion of the spatial units in terms of spatial information. Half of the units have a spatial information rate larger than 14 b/s. (b) Histogram of the information about head directions conveyed by spatial units. The directional information rate is close to zero. (c) Scatter plot of the spatial information rate and the direction information rate. Each dot represents one spatial unit. Spatial units conveyed far more information about location than about head direction.

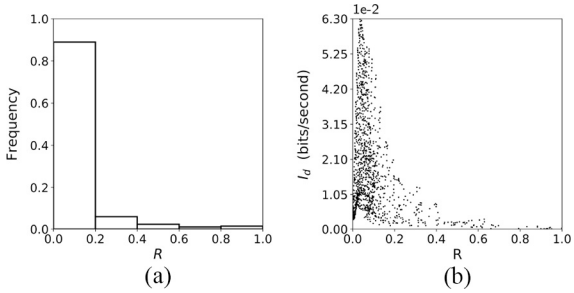

Fig. 7. Activity of spatial units is nonselective in head directions. (a) When assessed with the Rayleigh vector length R [ref. (18)], all spatial units have very low values, indicating no directional selectivity. (b) Scatter plot of the Rayleigh vector length and the directional information rate. Each dot represents one spatial unit. Both the direction selectivity and the head direction information conveyed by spatial units are low.

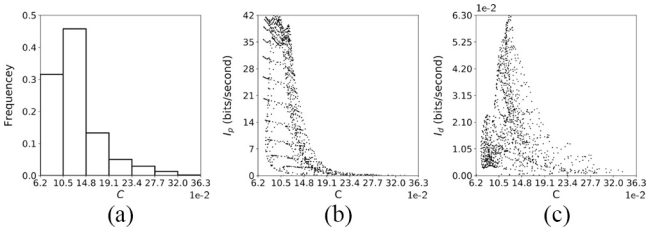

Fig. 8. Spatial codes of the spatial units are consistent across head directions. (a) Histogram of the consistency scores C [ref. (19)]. The consistency scores are approximately zero for all spatial units. (b) and (c) Scatter plots of the consistency score and the spatial information (b) and the directional information (c). Each dot corresponds to one unit. The distributions are widely scattered without any particular structure.

To measure the consistency of the firing maps in different head directions, we compute the consistency scores of the spatial units based on the KL divergence. The consistency scores of the spatial units are near zero [Fig. 8(a)]. In other words, the activity map of spatial units is consistent across different heading directions. The consistency score is not correlated to either the spatial information measure or the directional information measure [Fig. 8(b) and (c)], since their joint distributions are dispersed.

C. Position Prediction

The activity of spatial units provides a neural code of the locations in the environment. We construct a perceptron

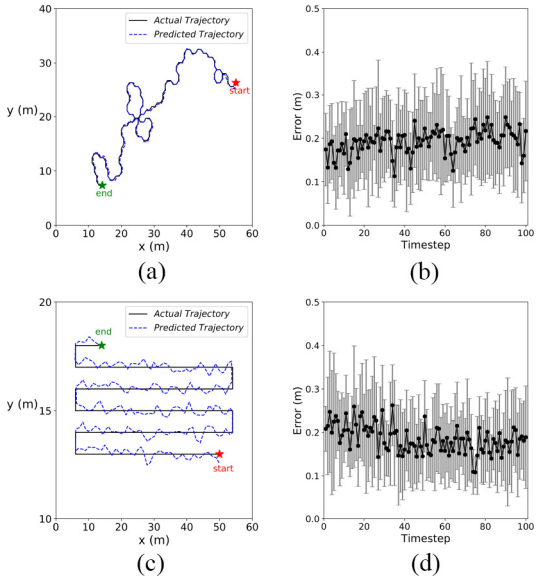

Fig. 9. Readout network can faithfully decode the trajectory of the robot, including the random exploration (a) and zig-zag traverse (c). (a) and (c) *Black line* shows an actual trajectory of the robot, while the *blue dashed line* indicates the corresponding predicted positions. (b) and (d) Mean position prediction errors of random exploration trajectories (b) and of zig-zag trajectories (d), averaged across ten different runs, respectively, from the activity of the SeMINet. Error bars indicate ± standard deviations. Only the first 100 time steps are shown for clarity, which manifest that the position prediction performance of SeMINet is not trajectory dependent.

network to decode the positional information from the activity of spatial units. After training in the learning phase, the readout units faithfully predict the actual position of the robot. The simulation then proceeds ten independent runs with random starting points to test the positional coding performance of the network. One example trajectory is shown in Fig. 9(a) and the mean prediction error (mean-squared error) across all runs stabilizes around 0.191 [Fig. 9(b)]. Moreover, the position prediction performance of SeMINet is not trajectory-dependent. The zig-zag moving pattern is also simulated [Fig. 9(c)], whose averaged prediction error stabilizes around 0.187 [Fig. 9(d)]. Therefore, the SeMINet could work as a positional encoding network from sensory inputs, and could support reward learning and other cognitive functions [48], such as decision making and memory consolidation.

D. Dynamics of the Network

The activity bump is the neural state of the network, and the center of the bump in the neural space encodes the position of the robot in the environment. When the robot moves in the environment and the velocity information is provided to the network, the network performs path integration to track the position of the robot. The activity bump of the network is shifted by the recurrent connections due to the asymmetry of the connection profile. We estimated the velocity of the bump according to the method described in Section II-E. During the simulation, the velocity components of the bump in the neural space are proportional to the actual velocity components of the robot in the environment [Fig. 10(a) and (b)]. This demonstrates that the network is able to faithfully track the position of the robot. Due to this linear relationship between

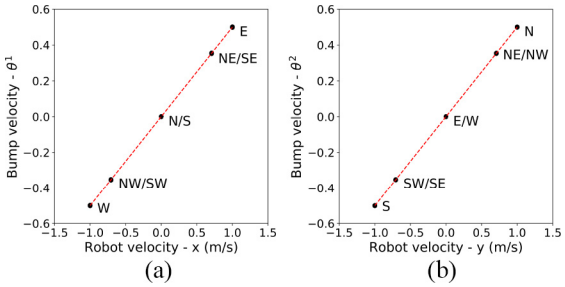

Fig. 10. Dynamics of the bump in the neural space during 20 000 steps of simulation. The velocities of the robot are shown in Table I. (a) Scatter plot of the velocity of the bump in the θ^1 dimension and the velocity of the robot in the x dimension of the environment. The relation between the two velocities can be fitted by a straight line (*red dashed line*) passing through the origin. The slope of the linear relation is equal to the parameter $S = 0.5$ s/m [ref. (4)]. (b) Velocity of the bump in the θ^2 dimension is linearly related to the velocity of the robot in the y dimension. The red dashed line is the linear fit.

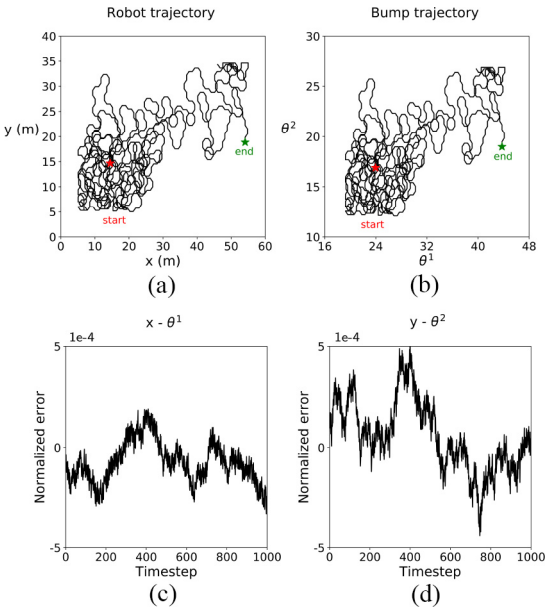

Fig. 11. Network performs path integration when the velocity stimulus and the visual stimulus are available. (a) Actual positions of the robot. The red star represents the starting position at the beginning of the test phase. (b) Estimated bump locations in the neural space (14). Red star is the initial location of the bump. (c) and (d) Positional differences between the normalized trajectory of the robot and the normalized trajectory of the bump are fluctuating around zero in x dimension (c) and y dimension (d).

the movement velocity in the environment and the bump velocity in the neural space, the positions of the environment are linearly mapped to the bump locations in the model. We thus test the SeMINet further and find that the locations of the robot in the environment are consistently encoded by the coordinates in the neural space [Fig. 11(a) and (b)]. After normalized in each space, respectively, the difference between the normalized robot locations and the normalized coordinates in the neural space fluctuates around zero [Fig. 11(c) and (d)].

E. Correction of the Motion Noise by Visual Inputs

The motion of the robot can be subject to errors. In the testing phase, we perturb the movement of the robot by adding motion noise from a uniform distribution in the

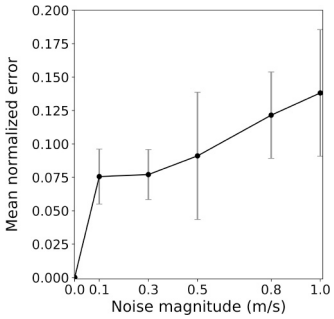

Fig. 12. Robustness of the network against motion noise. Mean Euclidean distances between the normalized robot trajectory and the normalized bump trajectory for different noise magnitudes.

range $[-U, U]$. The noise magnitudes are set to $U = 0, 0.1, 0.3, 0.5, 0.8,$ and 1 m/s, respectively. The error, calculated by the Euclidean distance between the normalized trajectories and the normalized activity bump positions of the robot, grows slowly with the increase of the motion noise (Fig. 12). The higher the trajectory error, the lower the positional decoding accuracy.

Fig. 13(a)–(f) shows the simulation when the noise magnitude $U = 0.5$ m/s, that is, 50% relative to the magnitude of the intended motion. The actual trajectory of the robot deviates from the planned trajectory [Fig. 13(a)]. The self-motion cues entering the network are not in accordance with the actual movements of the robot. Due to the learned connections between the visual units and the spatial units, the visual units can change the network states to compensate the mismatch between the actual motion and the intended motion cues. The bump trajectory is, therefore, twisted approaching the shape of the actual trajectory [Fig. 13(b)]. The linear relationship between the actual movements of the robot and the velocities of the activity bump is still preserved [Fig. 13(c) and (d)]. As a result, the errors between the normalized actual trajectory and the normalized bump trajectory are small [Fig. 13(e) and (f)]. Therefore, with visual inputs correcting path integration, the network accurately represents the current location of the robot even when the motion is perturbed by significant amounts of noise. This demonstrates the robustness of the network in maintaining spatial representations during movement.

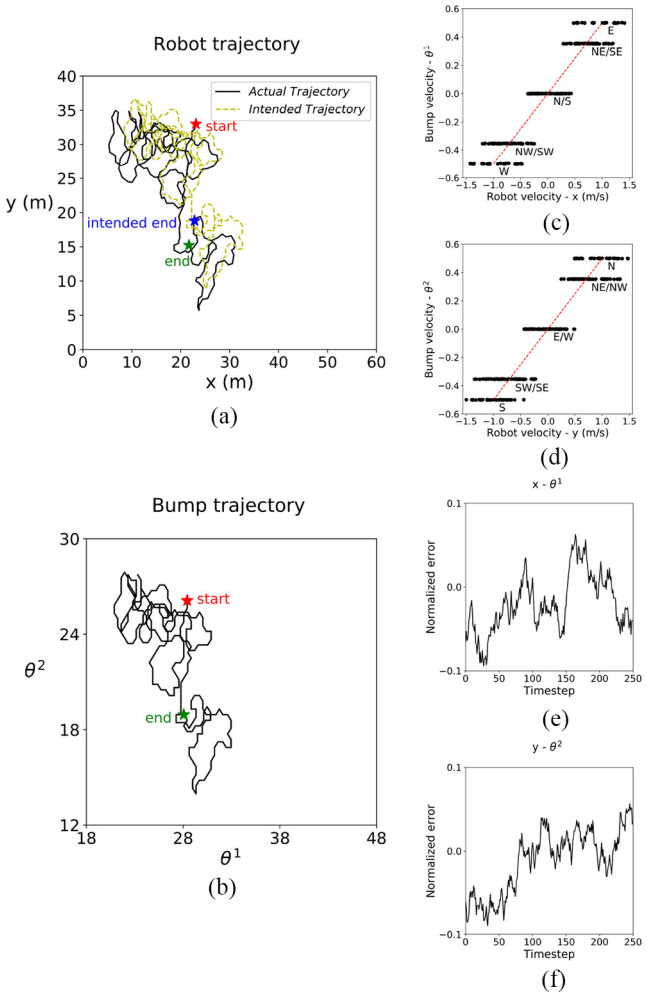

Fig. 13. Dynamics of the network against motion noise with magnitude $U = 0.5$ m/s. (a) Actual trajectory of the robot (*black line*) and its intended trajectory (*yellow dashed line*) in the environment during the testing phase. (b) Bump locations during the testing phase. (c) Scatter plot of the velocities of the bump in the θ^1 dimension and the velocities of the robot in the x dimension during the testing phase. The motion of the robot has random jitters, which are sampled from a uniform distribution in the range of $(-0.5, 0.5)$ m/s in both directions. The linear relationship between the actual velocities in the environment and the velocities of the bump is kept in spite of the motion noise. (d) Velocity of the bump in the θ^2 dimension is linearly related to the velocity of the robot in the y dimension. The linear relationship is robust against the perturbation in motion. (e) and (f) Difference between the normalized positions from the actual trajectory and the normalized bump locations in the neural space, shown separately for each dimension.

F. Relocalization by Visual Inputs

When the robot enters a familiar environment, or when it loses the track of its own positions, it needs to recover the correct internal representations of the locations, that is, relocalize [49]. Visual inputs serve an important source of cues for relocalization. In order to evaluate the relocalization ability of the SeMINet network, we teleport the robot to some location in the environment. To create a localization error, we initialize the bump activity of the spatial units in a location at a certain distance to the current location of the robot. Then the robot stays still, and the SeMINet network updates its internal representations through visual inputs and zero velocity [$\boldsymbol{a}(t) = 0$ in (4)]. We use a larger strength for visual inputs ($\rho = 50$) as compared to that during the learning phase to facilitate relocalization. Fig. 14(a) shows examples of the final bump locations in the neural space after relocalization. When there is no error introduced, the bump is maintained at the intended location. When the initial relocation error is introduced, the final bump locations no longer represent the correct location. On average, the localization error increases linearly with respect to the initial localization error [red line in Fig. 14(b)]. The error corrected by the network is relatively small compared to the initial relocation error [blue line in Fig. 14(b)]. This demonstrates that the network has limited ability in relocalization, but is able to correct small errors during locomotion as shown in Section IV-E.

Relocalization depends on both visual inputs and feedforward weights. The correlation between the activity patterns of the visual units at different locations in the environment

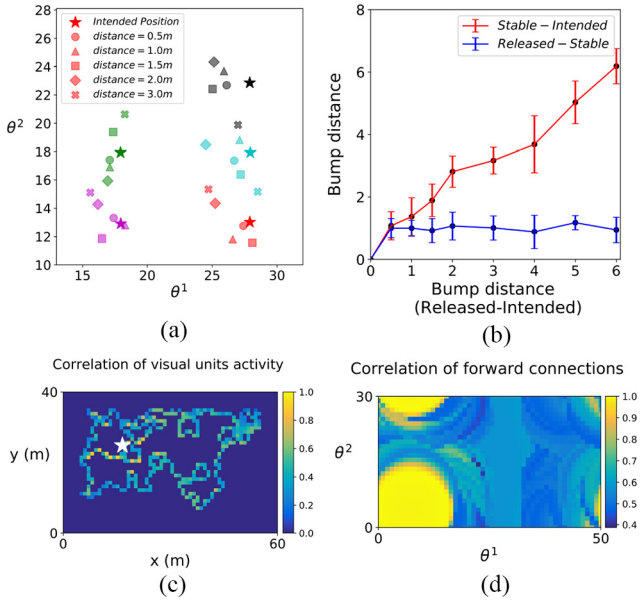

Fig. 14. Limited relocation performance of the network. The activity bump is first released in locations at a fixed distance to the correct location in the neural space, resulting in initial relocalization errors. The initial localization error is varied from 0 to 6 units (0–3 m) in the neural space. After 100 time steps, the bump stabilizes due to the attractor dynamics. (a) Locations of the final stable bumps. Five intended locations are shown by stars distinguished by colors. The final stable locations are shown by different markers. The magnitude of the initial localization error is represented by the shape of the marker. $\rho = 50$ [ref. (1)], all other parameters are the same with the standard values. (b) Errors remained and corrected during relocalization by visual inputs. *Red line* represents the average distance across trials between the final bump location and the intended bump location, that is, the error remained to be corrected. *Blue line* represents the distance across trials between the location of the initially released bump and the location of the final stable bump, that is, the error already corrected by the visual inputs. (c) Correlation between the activity of the visual units at the location marked by the *white star* and the activities of the visual units at other locations along the trajectory. The response of visual units is similar at multiple locations, resulting in high correlations. (d) Correlation between the feedforward weights of one example place units in the lower left region of the neural space with those of all other place units.

shows multiple peaks [Fig. 14(c)]. The activity of the visual units alone is, therefore, not sufficient to discriminate between different locations. The correlation between the feedforward weights of one place unit and those of all other place units is high for nearby units but low for units far away [Fig. 14(d)]. The high correlation in the feedforward weights between the units within short distance is a result of attractor states and Hebbian learning. The high correlation in the feedforward weights is one key factor leading to limited relocalization performance.

V. Discussion

A. Principle Findings

The primary goal of this article is to learn the cognitive map representations for a mobile robot. Based on the neurobiological findings in the neural circuits of visual perception and spatial cognition, we present a brain-inspired neural-network model to learn cognitive map representations by integrating sensory and motion information for robot navigation. Principle findings have confirmed that the activity of the spatial units in the model expresses positional coding of the robot in the environment, similar to the place fields of place cells observed in the hippocampus of rodents. The allocentric representations of the robot in the network can be decoded by a perceptron network with high decoding precision. The formation of the place codes depends critically on the neural dynamics of the network. The recurrent connections of the network produce and sustain an activity bump. Triggered by the internal self-motion cues, the activity bump is translated dynamically in the neural space in accordance with the motion of the robot, successfully transforming actual movement information into positional representations. The asymmetrical recurrent connections provide a neurobiologically plausible mechanism for path integration. The drift error in the motion is corrected by the association between the sensory information from the visual units and the network state of the spatial units. The integration of sensory and motor information leads to cognitive map representations with robustness against accumulated motion errors.

B. Related Work and Significance

Places cells in the dentate gyrus or the CA1 area of the hippocampus have been modeled to integrate the inputs from the EC [50]–[53]. These models do not consider path integration, and focus on the transformation from grid cells to place cells. Neurophysiological studies point to the ability of the hippocampus in forming the cognitive map by sensory-motor integration [32]. Some of the existing models are inspired by the path integrator idea. Müller *et al.* [14] proposed the "cognitive graph" model for encoding the transition between locations in the environment by learning connections between place cells. This model assumes that place cells have already formed place fields, and, therefore, does not account for the dynamic formation of place codes [38]. The idea of "cognitive graph" was elaborated in [15], and a multichart map-based path integrator (MPI) model was proposed. The MPI model introduces a motor system into the network and a path-integration subnetwork integrates the velocity by interacting with a place cell network. In the MPI model, the sensory information is simply modeled as ideal Gaussian functions. In our model, path integration is directly performed by place units due to the asymmetric recurrent connections, and the sensory information comes from visual images through the encoding of a deep neural network. Okeefe and Burgess [54] offered a model based on the stimulation of place cells only by visual representations [54]. Their model depends on the geometric information relative to the walls of the environment, and is not able to account for the existence of place fields in complete darkness where sensory cues are not robustly available. The vector-based navigation method using grid-like representation in artificial agents called the grid cell agent was developed in [21]. The grid cell agent uses place cells activity, simplified as a Gaussian pattern or learned from visual images, as one kind of supervised learning signals to train a path-integration model, in which entorhinal grid cells emerge. We, however, use an unsupervised and more biologically plausible model to perform the path integration by using the dynamical place coding of the CA3 subregion, the well-known structure for mammalian navigation. In addition, visual features, possibly

coming from LEC, in our model directly project to the path-integration module. This allows our model to integrate not only velocity information but also sensory information for robust spatial representation.

However, visual information extracted in this article is not discriminative enough to support the relocalization task. On the one hand, the VGG16 network, pretrained on the generic dataset for object recognition, is the visual module used to extract visual features from images in this article. The network has a fixed connection structure such that the size of input images has to be limited to 128 pixels $\times$ 128 pixels, resulting in much narrower FOV than that obtained in the previous study using input images of 320 pixels in width [27]. Small FOV in this article would lead to ambiguity in place recognition, especially, in environments without rich textures. The FOV of a rat can be as wide as 320°, and would gather enough visual information to complete one-to-one correspondence between visual cues and positions. One the other hand, unsupervised biologically plausible models, like VisNet in [31], could be used to learn visual features of higher expressive power for the navigation task.

Moreover, the resolution of place fields may also affect relocalization. Higher resolution would improve relocalization performance. Neurobiological findings reveal that hippocampal pyramidal cells of rodents form multiple place populations, with increasing place field resolution from ventral to dorsal [55]. Building multiresolutional cognitive map representations for natural environments is yet to investigate and determine the resulting advantage in relocalization.

Our architecture consists of a visual system representing features of the environment, a spatial memory system with recurrent connections encoding spatial information by sensory–motor integration, and a decoding layer to predict locations of the robot from spatial representations. In summary, there are three major contributions of this article. First, the sensory information is extracted by a deep neural network and this allows applying our model to real-world navigation tasks. Second, a competitive learning process establishes the association between the sensory representations and the memory state of the place units, and is able to correct the accumulated errors in the motion. Third, we develop quantitative measures of the activity of place units, revealing the coding properties in locations and head directions. These measures constitute objective indicators of the activity of both artificial neural networks and the neural circuits in the brain.

C. Future Work

In the model, the velocity inputs could come from the intended motion provided by the motor area. The optical flow from the visual scene is another important source of the movement information. It would give more robust movement estimation if a visual network is added to the model to extract velocities from the optical flow. Our model does not include head-direction cells, and assumes a limited range of movements. These aspects will be expanded by including a separate module of head-direction cells and mechanisms of short-term synaptic plasticity for movement integration.

We assume that the visual system has already developed, and adopt a pretrained deep neural network in the model. It would be interesting to model the development of the visual perception system together with the spatial memory system. More important, by training a deep neural network for the task of navigation, the responses of visual units would become better indicators of locations, and would support localization better.

Our model only includes a single population of spatial units. A more complete model needs to have multiple populations of place cells with the increasing resolutions of spatial coding. In addition, our model could be extended to include grid cells, which function later than place cells in the MEC during the postnatal development [56], [57]. Our expectation is that the grid cell network would increase the performance of path integration in the large-scale environment due to its multiresolution coding properties [58] and support vector-based navigation [21].

This article tries to bridge the gap between neurobiological findings and navigation models. The brain-inspired model presented in this article is a step toward more realistic algorithms for robot navigation in real-world environments. Thus, further work extending the proposed model to tackle actual robot navigation tasks should be taken into consideration. Navigation performance, efficiency, robustness as well as costs are all important indices to evaluate the proposed architecture in future research.

VI. Conclusion

The SeMINet model proposed in this article provides a unified model of perception and memory for the navigation task. The model generates memory states internally by its recurrent connections, and updates the memory states by integrating sensory–motor information. Competitive learning between the perception system and the memory system establishes the associations between the sensory cues in the environment and the memory states of the network, and allows the network to correct small drift errors caused by imperfect motions cues. The simulation results demonstrate that the network forms a cognitive map of the environment that is robust against the noise in the movement signal. The proposed SeMINet model, in the future, possibly provides a brain-inspired framework of cognitive maps for robots' navigation in realistic environments.

Appendix
Spatial Information of Place Cell Activity

The spatial information of a place cell is measured by the mutual information between its firing activity and spatial location [59]

$$I(S|X) = \sum_{x,s} p(s,x) \log_2 \frac{p(s,x)}{p(s)p(x)} \tag{21}$$

where X and S are discrete random variables representing spatial location and the spiking activity of the place cell, respectively. X is the binned location of the environment. $S \in \{0, 1\}$ is the state of the cell, with 0 and 1 corresponding

to the silence and spiking of the cell. $p(x)$ is the occupancy probability of the robot in location x.

The mutual information in (21) can be written as [42]

$$\begin{aligned} I(S|X) &= \sum_{x,s} p(s|x)p(x)\log_2\frac{p(s|x)}{p(s)} \\ &= \sum_x p(x)\Bigg[p(S=1|x)\log_2\frac{p(S=1|x)}{p(S=1)} \\ &\quad + (1-p(S=1|x))\log_2\frac{1-p(S=1|x)}{1-p(S=1)}\Bigg] \\ &\approx \sum_x p(x)\Bigg[p(S=1|x)\log_2\frac{p(S=1|x)}{p(S=1)} \\ &\qquad + \frac{1}{\ln 2}(1-p(S=1|x)) \\ &\qquad \times (-p(S=1|x)+p(S=1))\Bigg] \qquad (22) \\ &\approx \sum_x p(x)\Bigg[p(S=1|x)\log_2\frac{p(S=1|x)}{p(S=1)} \\ &\qquad + \frac{1}{\ln 2}(-p(S=1|x)+p(S=1))\Bigg] \qquad (23) \\ &= \sum_x p(x)p(S=1|x)\log_2\frac{p(S=1|x)}{p(S=1)}. \qquad (24) \end{aligned}$$

Equation (22) is obtained by the Talyor expansion of the function $\log_2(1-p)$ and neglecting the high-order terms. Equation (23) also neglects the high-order terms. $p(S=1|x)$ is the probability of a spike at location x. Equation (24) is derived by considering that fact that $p(S=1)=\sum_x p(S=1|x)p(x)$.

Assuming the spiking of a cell at location x is a Poisson process with mean $f(x)$, in small time interval Δt, the probability of a spike $p(S=1|x)$ can be written as

$$p(S=1|x) = f(x)\Delta t \qquad (25)$$

then, the mutual information in (24) reduces to

$$I(S|X) = \sum_x p(x)f(x)\Delta t\log_2\frac{f(x)}{\bar{f}} \qquad (26)$$

where $\bar{f}=\sum_x f(x)p(x)$ is the mean firing rate of the cell.

The information rate of the cell, that is, the spatial information per unit time, is

$$\begin{aligned} I &= \frac{I(S|X)}{\Delta t} \\ &= \sum_x p(x)f(x)\log_2\frac{f(x)}{\bar{f}}. \qquad (27) \end{aligned}$$

Assuming the occupancy probability $p(x)$ to be a uniform distribution, the information rate is given by

$$I_p = \frac{1}{N_p}\sum_x f(x)\log_2\frac{f(x)}{\bar{f}} \qquad (28)$$

where N_p is the number of location bins. Following the convention, $0\log_2 0$ is defined to be 0.

REFERENCES

[1] C. Petres, Y. Pailhas, P. Patron, Y. Petillot, J. Evans, and D. Lane, "Path planning for autonomous underwater vehicles," *IEEE Trans. Robot.*, vol. 23, no. 2, pp. 331–341, Apr. 2007.

[2] R. G. Golledge, "Human way finding and cognitive maps," in *The Colonization of Unfamiliar Landscapes*. London, U.K.: Routledge, 2003, pp. 49–54.

[3] A. Gagliardo, P. Ioalé, and V. P. Bingman, "Homing in pigeons: The role of the hippocampal formation in the representation of landmarks used for navigation," *J. Neurosci.*, vol. 19, no. 1, pp. 311–315, 1999.

[4] C. Cadena *et al.*, "Past, present, and future of simultaneous localization and mapping: Toward the robust-perception age," *IEEE Trans. Robot.*, vol. 32, no. 6, pp. 1309–1332, Dec. 2016.

[5] S. Thrun, W. Burgard, and D. Fox, *Probabilistic Robotics (Intelligent Robotics and Autonomous Agents Series)*. Cambridge, MA, USA: MIT Press, 2005.

[6] G. Dudes and M. Jenkin, *Computational Principles of Mobile Robotics*. Cambridge, U.K.: Cambridge Univ. Press, 2010.

[7] J. Zhang, L. Tai, J. Boedecker, W. Burgard, and M. Liu, "Neural SLAM: Learning to explore with external memory," 2017. [Online]. Available: arXiv:1706.09520.

[8] X. Gao and T. Zhang, "Unsupervised learning to detect loops using deep neural networks for visual SLAM system," *Auton. Robots*, vol. 41, no. 1, pp. 1–18, 2017.

[9] J. J. Knierim, "From the GPS to HM: Place cells, grid cells, and memory," *Hippocampus*, vol. 25, no. 6, p. 719, 2015.

[10] J. O'Keefe and J. Dostrovsky, "The hippocampus as a spatial map. Preliminary evidence from unit activity in the freely-moving RAT," *Brain Res.*, vol. 34, no. 1, pp. 171–175, 1971.

[11] J. Okeefe and L. Nadel, "The hippocampus as a cognitive map," *Amer. J. Psychol.*, vol. 93, no. 1, p. 177, 1978.

[12] E. C. Tolman, "Cognitive maps in rats and men," *Psychol. Rev.*, vol. 55, no. 4, pp. 189–208, 1948.

[13] S.-J. Zhang *et al.*, "Optogenetic dissection of entorhinal-hippocampal functional connectivity," *Science*, vol. 340, no. 6128, 2013, Art. no. 1232627.

[14] R. U. Müller, M. Stead, and J. Pach, "The hippocampus as a cognitive graph," *J. Gen. Physiol.*, vol. 107, no. 6, pp. 663–694, 1996.

[15] A. Samsonovich and B. L. McNaughton, "Path integration and cognitive mapping in a continuous attractor neural network model," *J. Neurosci.*, vol. 17, no. 15, pp. 5900–5920, 1997.

[16] A. Guazzelli, M. Bota, and M. A. Arbib, "Competitive Hebbian learning and the hippocampal place cell system: Modeling the interaction of visual and path integration cues," *Hippocampus*, vol. 11, no. 3, pp. 216–239, 2001.

[17] M. J. Milford and G. F. Wyeth, "Mapping a suburb with a single camera using a biologically inspired SLAM system," *IEEE Trans. Robot.*, vol. 24, no. 5, pp. 1038–1053, Oct. 2008.

[18] D. Sheynikhovich, R. Chavarriaga, T. Strösslin, A. Arleo, and W. Gerstner, "Is there a geometric module for spatial orientation? Insights from a rodent navigation model," *Psychol. Rev.*, vol. 116, no. 3, pp. 540–566, 2009.

[19] H. Tang, W. Huang, A. Narayanamoorthy, and R. Yan, "Cognitive memory and mapping in a brain-like system for robotic navigation," *Neural Netw.*, vol. 87, pp. 27–37, Mar. 2017.

[20] T. Zeng and B. Si, "Cognitive mapping based on conjunctive representations of space and movement," *Front. Neurorobot.*, vol. 11, p. 61, Nov. 2017.

[21] A. Banino *et al.*, "Vector-based navigation using grid-like representations in artificial agents," *Nature*, vol. 557, pp. 429–433, May 2018.

[22] D. J. Felleman and D. C. Van Essen, "Distributed hierarchical processing in the primate cerebral cortex," *Cerebr. Cortex*, vol. 1, no. 1, pp. 1–47, 1991.

[23] A. Arleo and W. Gerstner, "Spatial cognition and neuro-mimetic navigation: A model of hippocampal place cell activity," *Biol. Cybern.*, vol. 83, no. 3, pp. 287–299, 2000.

[24] J. Conklin and C. Eliasmith, "A controlled attractor network model of path integration in the rat," *J. Comput. Neurosci.*, vol. 18, no. 2, pp. 183–203, 2005.

[25] R. P. Rao, "Bayesian computation in recurrent neural circuits," *Neural Comput.*, vol. 16, no. 1, pp. 1–38, 2004.

[26] W.-H. Zhang and S. Wu, "Reciprocally coupled local estimators implement Bayesian information integration distributively," in *Proc. 26th Adv. Neural Inf. Process. Syst.*, 2013, pp. 19–27.

[27] M. Franzius, H. Sprekeler, and L. Wiskott, "Slowness and sparseness lead to place, head-direction, and spatial-view cells," *PLoS Comput. Biol.*, vol. 3, no. 8, p. e166, 2007.
[28] S. S. Deshmukh and J. J. Knierim, "Representation of non-spatial and spatial information in the lateral entorhinal cortex," *Front. Behav. Neurosci.*, vol. 5, p. 69, Oct. 2011.
[29] M. E. Hasselmo, E. T. Rolls, G. C. Baylis, and V. Nalwa, "Object-centered encoding by face-selective neurons in the cortex in the superior temporal sulcus of the monkey," *Exp. Brain Res.*, vol. 75, no. 2, p. 417, 1989.
[30] N. C. Aggelopoulos, L. Franco, and E. T. Rolls, "Object perception in natural scenes: Encoding by inferior temporal cortex simultaneously recorded neurons," *J. Neurophysiol.*, vol. 93, no. 3, pp. 1342–1357, 2005.
[31] L. Robinson and E. T. Rolls, "Invariant visual object recognition: Biologically plausible approaches," *Biol. Cybern.*, vol. 109, no. 4, pp. 505–535, 2015.
[32] T. L. Bjerknes, N. C. Dagslott, E. I. Moser, and M. B. Moser, "Path integration in place cells of developing rats," *Proc. Nat. Acad. Sci. USA*, vol. 115, no. 7, pp. E1637–E1646, 2018.
[33] G. J. Quirk, R. U. Müller, and J. L. Kubie, "The firing of hippocampal place cells in the dark depends on the rat's recent experience," *J. Neurosci.*, vol. 10, no. 6, pp. 2008–2017, 1990.
[34] E. J. Markus, C. A. Barnes, B. L. Mcnaughton, V. L. Gladden, and W. E. Skaggs, "Spatial information content and reliability of hippocampal CA1 neurons: Effects of visual input," *Hippocampus*, vol. 4, no. 4, pp. 410–421, 1994.
[35] S. Leutgeb, J. K. Leutgeb, C. A. Barnes, E. I. Moser, B. L. Mcnaughton, and M. B. Moser, "Independent codes for spatial and episodic memory in hippocampal neuronal ensembles," *Science*, vol. 309, no. 5734, pp. 619–623, 2005.
[36] S. Leutgeb, J. K. Leutgeb, M. B. Moser, and E. I. Moser, "Place cells, spatial maps and the population code for memory," *Current Opin. Neurobiol.*, vol. 15, no. 6, pp. 738–746, 2005.
[37] J. O'Keefe, "Place units in the hippocampus of the freely moving rat," *Exp. Neurol.*, vol. 51, no. 1, pp. 78–109, 1976.
[38] M. A. Wilson and B. L. Mcnaughton, "Dynamics of the hippocampal ensemble code for space," *Science*, vol. 261, no. 5124, pp. 1055–1058, 1993.
[39] B. L. Mcnaughton, F. P. Battaglia, O. Jensen, E. I. Moser, and M. B. Moser, "Path integration and the neural basis of the 'cognitive map,"' *Nat. Rev. Neurosci.*, vol. 7, no. 8, pp. 663–678, 2006.
[40] M. Tsodyks and T. Sejnowski, "Associative memory and hippocampal place cells," *Int. J. Neural Syst.*, vol. 6, pp. 81–86, 1995.
[41] E. T. Rolls, "Invariant visual object and face recognition: Neural and computational bases, and a model, VisNet," *Front. Comput. Neurosci.*, vol. 6, no. 2, p. 35, 2012.
[42] W. E. Skaggs, B. L. Mcnaughton, and K. M. Gothard, "An information-theoretic approach to deciphering the hippocampal code," in *Proc. Adv. Neural Inf. Process. Syst.*, 1992, pp. 1030–1037.
[43] P. Berens, "CircStat: A MATLAB toolbox for circular statistics," *J. Stat. Softw.*, vol. 31, no. 10, pp. 1–21, 2009.
[44] F. Schoenfeld and L. Wiskott, "RatLab: An easy to use tool for place code simulations," *Front. Comput. Neurosci.*, vol. 7, no. 1, p. 104, 2013.
[45] S. I. Amari, "Dynamics of pattern formation in lateral-inhibition type neural fields," *Biol. Cybern.*, vol. 27, pp. 77–87, Jun. 1977.
[46] F. Stella, E. Cerasti, B. Si, K. Jezek, and A. Treves, "Self-organization of multiple spatial and context memories in the hippocampus," *Neurosci. Biobehav. Rev.*, vol. 36, no. 7, pp. 1609–1625, 2012.
[47] P. Lipton and H. Eichenbaum, "Complementary roles of hippocampus and medial entorhinal cortex in episodic memory," *Neural Plasticity*, vol. 2008, Jul. 2008, Art. no. 258467.
[48] N. J. Gustafson and N. D. Daw, "Grid cells, place cells, and geodesic generalization for spatial reinforcement learning," *PLoS Comput. Biol.*, vol. 7, no. 10, 2011, Art. no. e1002235.
[49] S. P. Engelson and D. V. Mcdermott, "Error correction in mobile robot map learning," in *Proc. IEEE Int. Conf. Robot. Autom.*, 1992, pp. 2555–2560.
[50] T. Solstad, E. I. Moser, and G. T. Einevoll, "From grid cells to place cells: A mathematical model." *Hippocampus*, vol. 16, no. 12, pp. 1026–1031, 2006.
[51] E. T. Rolls, S. M. Stringer, and T. Elliot, "Entorhinal cortex grid cells can map to hippocampal place cells by competitive learning," *Netw. Comput. Neural Syst.*, vol. 17, no. 4, pp. 447–465, 2006.
[52] B. Si and A. Treves, "The role of competitive learning in the generation of DG fields from EC inputs," *Cogn. Neurodyn.*, vol. 3, no. 2, pp. 177–187, 2009.
[53] S. Cheng and L. M. Frank, "The structure of networks that produce the transformation from grid cells to place cells," *Neuroscience*, vol. 197, no. 197, pp. 293–306, 2011.
[54] J. Okeefe and N. Burgess, "Geometric determinants of the place fields of hippocampal neurons," *Nature*, vol. 381, no. 6581, pp. 425–428, 1996.
[55] M. Jung, S. Wiener, and B. McNaughton, "Comparison of spatial firing characteristics of units in dorsal and ventral hippocampus of the rat," *J. Neurosci.*, vol. 14, no. 12, pp. 7347–7356, 1994.
[56] R. F. Langston *et al.*, "Development of the spatial representation system in the rat," *Science*, vol. 328, no. 5985, pp. 1576–1580, 2010.
[57] T. J. Wills, F. Cacucci, N. Burgess, and J. O'Keefe, "Development of the hippocampal cognitive map in pre-weanling rats," *Science*, vol. 328, no. 5985, p. 1573, 2010.
[58] S. Liu, B. Si, and Y. Lin, "Self-organization of hippocampal representations in large environments," in *Proc. Int. Joint Conf. Neural Netw.*, 2015, pp. 1–6.
[59] T. M. Cover and J. A. Thomas, *Elements of Information Theory (Wiley Series in Telecommunication and Signal Process)*. Hoboken, NJ, USA: Wiley-Intersci., 2017.

Dongye Zhao received the B.S. degree in detection guidance and control techniques from Central South University, Changsha, China. She is currently pursuing the Ph.D. degree with the State Key Laboratory of Robotics, Shenyang Institute of Automation, Chinese Academy of Sciences, Shenyang, China.

Her research interests include deep learning and computational neuroscience.

Zheng Zhang received the Ph.D. degree in electrical and computer engineering from the University of Illinois at Urbana–Champaign, Urbana, IL, USA.

He was a project lead and a Member of Technical Staff with HP-Labs, Palo Alto, CA, USA. He was the Founder of the System Research Group, Microsoft Research Asia, Beijing, China, where he served as a Principle Researcher and a Research Area Manager. He is a Professor of computer science with New York University Shanghai, Shanghai, China, and a Global Network Professor with New York University, New York, NY, USA. As of 2018, he is taking a leave of absence and has joined Amazon AWS, Seattle, WA, USA, taking the role of the Director of AWS Shanghai AI Lab, Shanghai. His research interests are theories and practices of large-scale distributed computing and its intersection with machine learning, in particular deep learning.

Hong Lu (Member, IEEE) received the B.Eng. and M.Eng. degrees in computer science and technology from Xidian University, Xi'an, China, and the Ph.D. degree from Nanyang Technological University, Singapore.

From 1993 to 2000, she was a Lecturer and a Researcher with the School of Computer Science and Technology, Xidian University. From 2000 to 2003, she was a Research Student with the School of Electrical and Electronic Engineering, Nanyang Technological University. Since 2004, she has been with the School of Computer Science, Fudan University, Shanghai, China, where she is currently a Professor. Her current research interests include image and video processing, computer vision, machine learning, and pattern recognition.

Sen Cheng received the Ph.D. degree in physics from Michigan State University, East Lansing, MI, USA.

He is a Professor with the Institute for Neuroinformatics, Ruhr-Universität Bochum, Bochum, Germany. He does research in computational neuroscience, focusing on the cognitive and neural mechanisms underlying episodic memory and spatial navigation.

Dr. S. Cheng is a Professor of computational neuroscience with the Institute for Neural Computation, Ruhr-Universität Bochum, Bochum, Germany. He studies the neural and cognitive mechanisms of episodic memory and spatial navigation using a variety of computational methods, such as biological neural networks, cognitive modeling, and machine learning. He founded and currently heads the DFG-funded research unit FOR 2812 "Constructing scenarios of the past: A new framework in episodic memory." His research is interdisciplinary and combines philosophical, psychological, neuroscientific, and computational aspects.

Bailu Si (Member, IEEE) received the Ph.D. degree in neurophysics from the University of Bremen, Bremen, Germany.

He was a Researcher with the State Key Laboratory of Robotics, Shenyang Institute of Automation, Chinese Academy of Sciences, Shenyang, China. He is a Professor with the Brain and Autonomous Intelligent Robots Lab, School of Systems Science, Beijing Normal University, Beijing, China. His research interests include intelligent robotics, machine learning, and computational neuroscience.

Xisheng Feng received the B.S. degree from the Harbin Institute of Technology, Harbin, China, in 1965.

He is a Senior Researcher with the Underwater Robots Laboratory, Shenyang Institute of Automation, Chinese Academy of Sciences, Shenyang, China. As a pioneer of underwater robots in China, he began to design and develop the underwater vehicles in 1982. His current research interests include marine robotics, acoustic image processing, and intelligent control.

Dr. X. Feng was elected as an Academician of the Chinese Academy of Engineering in 1999.